Hexagons, Kinks, and Disorder in Oscillated Granular Layers

Francisco Melo*

Departamento de Física, Universidad de Santiago, Avenida Ecuador 3493, Casilla 307 Correo 2, Santiago, Chile

Paul B. Umbanhowar[†] and Harry L. Swinney[‡]

Center for Nonlinear Dynamics and Department of Physics, The University of Texas at Austin, Austin, Texas 78712

Experiments on vertically oscillated granular layers in an evacuated container reveal a sequence of well-defined pattern bifurcations as the container acceleration is increased. Period doublings of the layer center of mass motion and a standing wave instability interact to produce hexagons and more complicated patterns composed of distinct spatial domains of different relative phase separated by kinks (phase discontinuities). A simple model displays quantitative agreement with the observed transition sequence.

The transport, mixing, and segregation of granular materials is important in industries ranging from food to mineral processing, yet a basic understanding of the physical mechanisms underlying the collective dynamics of grains is lacking. Recent experiments on vertically vibrated granular materials show a variety of phenomena including heap formation and convection [1,2], size segregation [3], and traveling waves [4]. These phenomena, although of practical importance, are caused by surrounding gas and/or sidewall driving [5], leaving open the question of whether there is any intrinsic self-organized behavior in these systems. We report here robust patterns that arise spontaneously, not from interstitial gas or sidewall forcing, but from correlations induced by multiple collisions between the grains and by the coherent motion of the particle layer and the container.

Our experiments on vertically vibrated granular layers yield spatial patterns composed of standing waves that oscillate at either one-half or one-quarter of the drive frequency f. Spatial domains of different relative phase separated by phase discontinuities (kinks) appear in all patterns except those just beyond the initial instability. Examples of stripes, squares, hexagons, kinks, and a disordered state are presented in Fig. 1. Figure 2 shows the stability region for each pattern as a function of f and the dimensionless acceleration amplitude $\Gamma = 4\pi^2 f^2 A/g$, where $2A$ is the peak-to-peak amplitude of the sinusoidal displacement of the container and g is the gravitational acceleration. The transitions are well defined, only weakly dependent on f, and nonhysteretic (except for the transitions to squares). We will now describe the experimental methods and then show how the patterns and their associated thresholds arise from the interaction of two distinct mechanisms: a standing wave instability [6,7] and period doublings.

A layer of 0.15–0.18 mm diameter bronze spheres is placed in the bottom of a cylindrical container that has inner diameter 127 mm and height 90 mm; the wall and lid are Lucite while the base is aluminum to reduce electrostatic effects. The layer is 7 particles deep except for the

data shown in Fig. 3, where a thicker layer (12 particles deep) improves the signal-to-noise ratio for the acceleration measurements. The container is evacuated to 0.1 Torr,
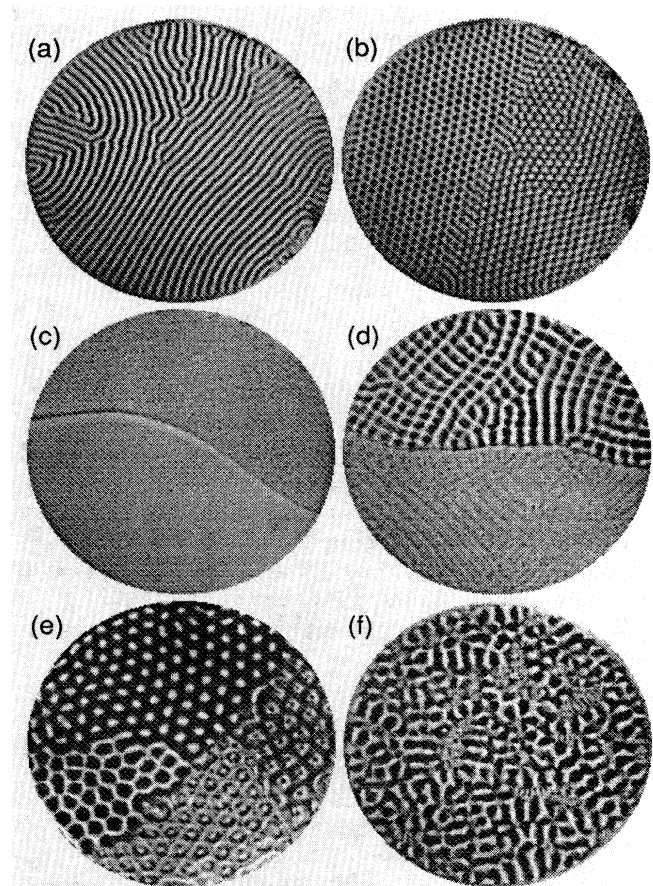

FIG. 1. Patterns in a 1.2 mm deep layer at $f = 67$ Hz: (a) $f/2$ stripes ($\Gamma = 3.3$), (b) $f/2$ hexagons ($\Gamma = 4.0$), (c) flat with kink ($\Gamma = 5.8$), (d) competing $f/4$ squares and stripes ($\Gamma = 6.0$), (e) $f/4$ hexagons ($\Gamma = 7.4$), and (f) disorder ($\Gamma = 8.5$).
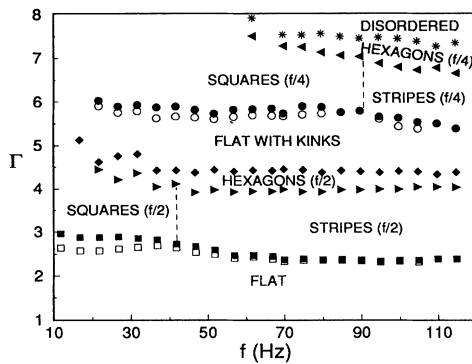
FIG. 2. Stability diagram showing transitions in a 1.2 mm deep layer. The vertical dashed lines indicate the frequencies above which only stripes appear in the square or stripe regime. Closed (open) square and circular symbols denote transitions with increasing (decreasing) Γ.
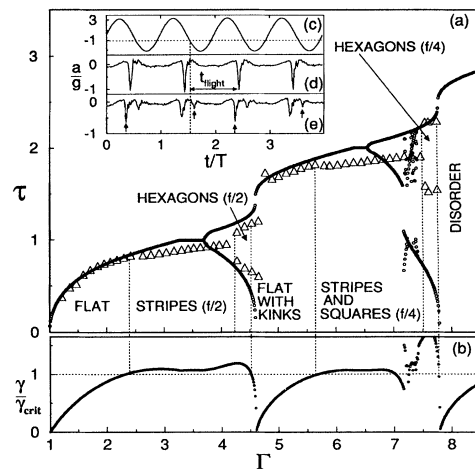

FIG. 3. Comparison of observations for a particle layer to calculations for a model consisting of a 1D completely inelastic ball. (a) Flight times for the layer (1.9 mm deep, $f = 67$ Hz), τ_{expt} ($\triangle$), and for a completely inelastic ball, τ_{calc} ($\bigcirc$). (b) The dimensionless layer collision acceleration γ/γ_{crit} (the average value is displayed where γ is multivalued). (c) Container acceleration (collisions removed). (d),(e) Impact acceleration for stripes ($\Gamma = 3.3$) and hexagons ($\Gamma = 4.2$), respectively (vertical arrows indicate successive collisions of regions with the same relative phase).

a value at which the volumetric effects of the gas are negligible [5] and heaping is not observed. An electromechanical vibration exciter drives the container, and the resulting acceleration is measured to a resolution of $0.01g$. Patterns are illuminated at low angle with a strobe light and are recorded with a video camera located above the container.

The instabilities leading to the different patterns can be understood in terms of two dimensionless parameters that characterize the dynamics of the layer: $\tau = f t_{flt}$, the layer free-flight time, and $\gamma = v_c/g t_{flt}$, which is approximately the acceleration of the granular layer relative to the plate during the time of collision (v_c is the relative collision velocity) [8]. We directly measure τ, while we deduce γ from a simple one-dimensional (1D) model of an inelastic ball on an oscillating plate. Figures 3(a) and 3(b) show the dependence of τ and γ on the driving acceleration Γ, and Table I indicates how the patterns can be characterized by the values of τ and γ/γ_{crit}, where γ_{crit} marks the onset of standing waves.

In our model system the ball is completely inelastic, because the collisions of the particle layer and container are almost completely inelastic due to multiple internal grain collisions. The ball motion is computed [9] by assuming that free flights begin whenever the ball and plate are in contact and the plate acceleration $a(t) < -g$. Figure 3(a) compares the calculated flight time τ_{calc} with the measured flight time τ_{expt} as a function of Γ. [Figures 3(c) and

3(d) indicate how τ_{expt} is measured.] In the absence of standing waves, the layer and ball motions are nearly the same: $\tau_{expt} = \tau_{calc}$. When standing waves are present the layer is dilated at takeoff, which reduces the effective takeoff velocity of the layer and consequently decreases τ_{expt}. Since γ is calculated from model values of v_c and t_{flt}, it is only accurate when standing waves are absent ($\gamma < \gamma_{crit}$). Because v_c and t_{flt} are both proportional to $1/f$, γ is independent of f; this is consistent with Fig. 2, which shows that the standing wave transitions depend only weakly on f.

For $\Gamma > 1$, on each cycle the layer loses contact and later collides with the container. However, it is not until $\Gamma \approx 2.4$ that the standing wave instability first occurs ($\gamma = \gamma_{crit}$) and the flat layer bifurcates to wave patterns oscillating at $f/2$, as shown in Fig. 1(a) [10]. Vertical lines extending from Fig. 3(a) to Fig. 3(b) mark the experimental values of Γ where transitions associated with the standing wave instability occur. The patterns are squares

TABLE I. Patterns and their associated instabilities.

Pattern	Instability	τ_{expt}	γ/γ_{crit}
Flat	None	<1	<1
$f/2$ squares or stripes	Wave	<1	>1
$f/2$ hexagons[a]	Wave and period-2	>, <1	>1
Flat with kinks	Period-2	>1	<1
$f/4$ squares or stripes	Wave and period-2	>1	>1
$f/4$ hexagons[a]	Wave and period-4	>, <2	>1

[a]Effective two-frequency forcing.

for $f < 24$ Hz and stripes for $f > 40$ Hz (Fig. 2); at intermediate values of f, both patterns compete. For squares the difference between the stability threshold for increasing and decreasing Γ is about 20%, while for stripes the hysteresis is small and perhaps even zero.

Hexagonal patterns arise spontaneously from squares or stripes when the vertical motion of the layer undergoes a period doubling bifurcation. Period doubling occurs when τ_{expt} exceeds unity and subsequently becomes double valued [see Fig. 3(a)]. As Fig. 3(e) shows, alternate collisions now occur before and after $a_c = -g$; the layer is effectively forced at both f and $f/2$ because successive collisions occur with different v_c and t_{flt}. Like squares and stripes, hexagonal patterns return to the same configuration after two periods but with an important difference: time translation by one period is no longer equivalent to a spatial shift of one-half wavelength. Instead, two distinct patterns appear in alternate cycles—a set of isolated peaks on a triangular lattice become, on the next oscillation, hexagonal cells, each one centered on a former peak location. The amplitude of the cellular phase is maximum at the end of the long flight, while the amplitude of the peaked phase is maximum at the end of the short flight. Figure 2 shows that the Γ value for transition to hexagons ($\Gamma \approx 3.9$) is nearly constant for frequencies above where the square or striped patterns show a strong decrease in hysteresis.

Spatial kinks separating domains of different relative phase appear at the period doubling bifurcation. Kinks arise because the period doubled motion is degenerate by π in phase: a portion of the layer can begin its motion on one cycle or the next. For hexagons, this degeneracy manifests itself in the simultaneous appearance of both peaked and cellular spatial domains separated by a well-defined phase defect, as shown in Fig. 1(b).

As Γ is increased further, the amplitude of the hexagonal pattern decreases until $\gamma/\gamma_{crit} < 1$ and standing waves disappear. The layer now consists of flat domains connected by a kink, as shown in Fig. 1(c). Physically, this resonance corresponds to $v_c \approx 0$: the layer lands gently on the plate. Flat domains with kinks arise solely from the period doubling instability and appear to be the 2D analog of the 1D subharmonic instability in a glass bead layer reported by Douady, Fauve, and Laroche [11].

Beyond onset of the flat domains with kinks, τ_{expt} is double valued as for the hexagonal patterns, but as Γ is increased the time of the shorter flight goes to zero and τ_{expt} again becomes single valued. In both cases the motion is period doubled: In the former, flights are composed of long and short jumps (effective two-frequency forcing), while in the latter, flights can begin on one cycle or the next, but the time between successive collisions is always $2/f$. In this latter state, $\tau_{expt} \approx \tau_{calc}$, indicating that the layer is compact at takeoff.

Square and striped patterns reappear when again $\gamma/\gamma_{crit} > 1$ at $\Gamma \approx 5.7$. Because the time between collisions is two periods the standing waves oscillate at

$f/4$ and, as Fig. 1(d) shows, appear in separate domains whose motions differ in phase by π (one domain is taking off while the other is in midflight). Otherwise $f/4$ squares and stripes are the same as their $f/2$ counterparts: the transition is accompanied by a decrease in τ_{expt} with respect to τ_{calc}, and squares appear subcritically at lower f, while at higher f stripes occur essentially without hysteresis.

Although the layer motion is period doubled for $f/4$ squares and stripes, hexagons do not appear because τ_{expt} is single valued; the layer experiences the same conditions on consecutive collisions. However, when $\tau_{expt} > 2$, the layer motion undergoes a second period doubling— effective two-frequency forcing (now at $f/2$ and $f/4$) is restored and hexagons reappear. Figure 1(e) shows that four different phases simultaneously exist in the system; each phase present before the second period doubling supports two separate phase domains of hexagons. As Fig. 2 indicates, the transition to $f/4$ hexagons is apparently nonhysteretic.

The layer becomes spatially and temporally disordered for $\Gamma \approx 7.6$. Disorder is introduced by circular regions approximately three cells in diameter, which randomly appear in the hexagonal patterns and then shrink and disappear over the course of approximately $50/f$. The circular regions are $\pi/4$ out of phase with the domain that contains them and result from a single flight of $t_{flt} \approx 1/f$, instead of $t_{flt} \approx 2/f$ as for the rest of the domain. For $\Gamma < 7.8$ the four phase domains associated with the hexagonal pattern remain intact. However, for larger Γ, hexagons and the boundaries between the stable domains disappear; the layer consists of numerous small domains of wavelike structures with short spatial and temporal correlation [see Fig. 1(f)]. The disordered state persists up to $\Gamma = 14$, the largest forcing examined.

The ordered patterns we observe in granular media have similarities with those in vertically oscillated fluids (Faraday experiment) [12], but an important difference is that period doubling, which is not observed in fluids, leads to domains with different phase in the granular layer. With this exception, it appears that the factors determining pattern selection in the two media are similar even though, because of free flights and collisions, the effective forcing of the granular layer is different from the smooth parametric forcing of the fluid. Dilation of the granular layer appears to be analogous to the inverse of viscosity in fluids because in the granular system we observe $f/2$ squares for large dilation and stripes for small dilation, while in fluids squares are observed for small viscosity (less than 0.7 cm^2/s) and stripes for large viscosity [12]. In the Faraday experiment hexagons appear when the container is externally driven simultaneously at both f and $f/2$, but only for certain ranges of the relative phase and amplitude of the two drive signals; if the phase difference is too small, squares are observed [13]. Hexagons appear in the granular layer when the intrinsic relative phase associated with the effective two-frequency

forcing is large. In thinner particle layers the transition to effective two-frequency forcing occurs for smaller Γ; consequently, the relative phase between long and short flights is smaller, and we observe patterns of squares with the same peak and cell structure as for hexagons.

The pattern formation phenomena we have described result from the interaction of standing waves and period doublings [14]. These mechanisms are characterized by the collisional acceleration and the dimensionless flight time, respectively, both of which can be calculated from a 1D model. We emphasize that the formation of the granular standing waves depends primarily on the relative collision velocity and is only indirectly a function of the acceleration amplitude Γ. In addition to the results reported here, we have performed experiments varying the particle restitution coefficient (0.5–0.95), density 2.3–11.4 $g\,cm^{-3}$, and size (0.05–3 mm); the layer thickness (2–40 particles) and aspect ratio (2–100); and the pressure (10^{-1}–10^{-6} Torr). No qualitative changes in the patterns or their associated bifurcations were observed. Moreover, in contrast with most other cooperative dynamic phenomena in granular systems, we have found that transition thresholds and pattern organization become better defined as the pressure is reduced and the ratio of container size to pattern wavelength is increased; this indicates that interstitial gas and sidewall forcing do not organize the grain motion. Future work examining basic transport properties such as viscosity and momentum diffusivity in the robust patterns we have found should have practical consequences.

*Electronic address: fmelo@lauca.usach.cl
†Electronic address: pbu@chaos.ph.utexas.edu
‡Electronic address: swinney@chaos.ph.utexas.edu

[1] P. Evesque and J. Rajchenbach, Phys. Rev. Lett. **62**, 44 (1989).

[2] C. Laroche, S. Douady, and S. Fauve, J. Phys. (Paris) **50**, 699 (1989).

[3] J. B. Knight, H. M. Jaeger, and S. R. Nagel, Phys. Rev. Lett. **70**, 3728 (1993).

[4] H. K. Pak and R. P. Behringer, Phys. Rev. Lett. **71**, 1832 (1993).

[5] H. K. Pak, E. Van Doorn, and R. P. Behringer, Phys. Rev. Lett. **74**, 4643 (1995).

[6] S. Fauve, S. Douady, and C. Laroche, J. Phys. (Paris) **50**, Suppl. 3, 187 (1989).

[7] F. Melo, P. Umbanhowar, and H. L. Swinney, Phys. Rev. Lett. **72**, 172 (1994).

[8] The form of γ is not critical. A better approximation is $\gamma = v_c/gt_{\text{flt}}[1 - (1 - \epsilon)gt_p/2v_c]$, where ϵ is the coefficient of restitution and t_p is the time spent on the plate; when t_p/v_c is small the expression in the text is recovered.

[9] For an analysis of the completely inelastic ball see A. Mehta and J. M. Luck, Phys. Rev. Lett. **65**, 393 (1990).

[10] Instability is thought to arise from two counterpropagating fluxes [7]. At onset in air with glass beads $\Gamma \approx 3.3$, while in vacuum $\Gamma \approx 2.8$. The strong increase in critical Γ in air near $f = 40$ Hz [7] is not observed in vacuum. See B. Thomas, M. O. Mason, Y. A. Liu, and A. M. Squires, Powder Technol. **57**, 267 (1989), for a description of other layer states observed in air.

[11] S. Douady, S. Fauve, and C. Laroche, Europhys. Lett. **8**, 621 (1989).

[12] W. S. Edwards and S. Fauve, J. Fluid Mech. **278**, 123 (1994).

[13] H. W. Müller, Phys. Rev. Lett. **71**, 3287 (1993).

[14] The two period doublings we observe experimentally are not associated with a Feigenbaum period doubling sequence.
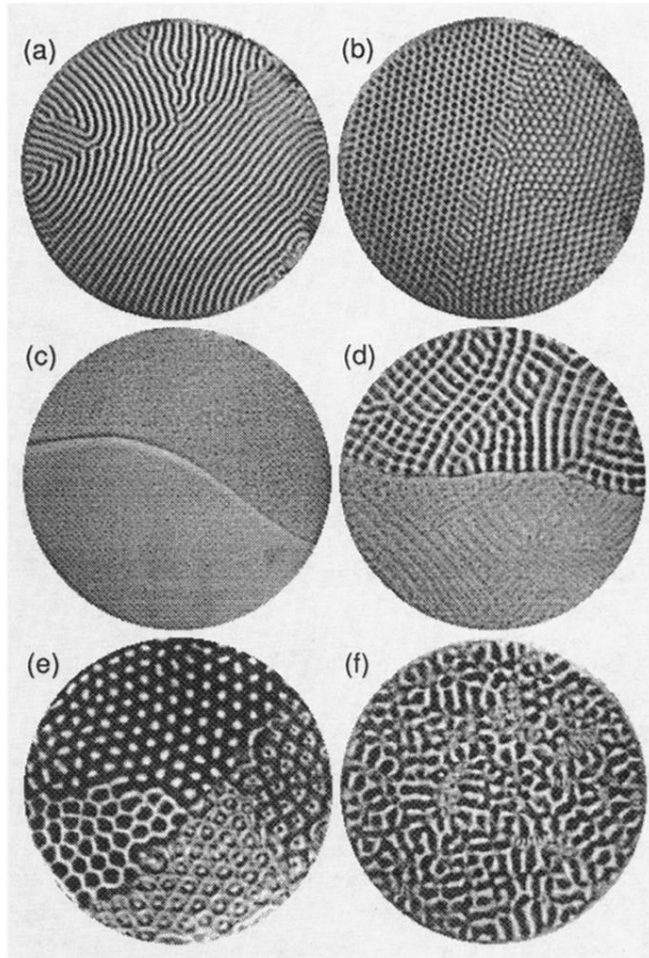
FIG. 1. Patterns in a 1.2 mm deep layer at $f = 67$ Hz: (a) $f/2$ stripes ($\Gamma = 3.3$), (b) $f/2$ hexagons ($\Gamma = 4.0$), (c) flat with kink ($\Gamma = 5.8$), (d) competing $f/4$ squares and stripes ($\Gamma = 6.0$), (e) $f/4$ hexagons ($\Gamma = 7.4$), and (f) disorder ($\Gamma = 8.5$).